Guidance, Navigation and Control for the autonomous rendezvous and docking of cooperative targets

A. Martinez [(1)], J. Ramirez [(1)], F. Cacciatore [(1)], P. Gonzalez [(1)]

[(1)] SENER Aerospace, Calle de Severo Ochoa, 4, 28760 Tres Cantos, Madrid (Spain)
alvaro.martinez@aeroespacial.sener

ABSTRACT

The relevance of In-Orbit Logistic missions for sustainable space exploration is growing exponentially. These missions pose tight requirements on the performance of the GNC subsystem and on the autonomy level for the operation of the spacecraft. In this framework, SENER Aerospace is developing Rendezvous and Docking GNC technologies based on onboard optimization, with the aim of increasing the flexibility, performance, and reliability of these missions. Such techniques are already being implemented in the frame of ESA In-Space Logistics Proof-of-Concept 1 mission studies.

This contribution presents a rendezvous GNC solution based on onboard convex optimization and optical navigation. The GNC is designed to ensure compatibility with the SIROM capture requirements, in order to guarantee the feasibility of the mating scenario. Several rendezvous and capture scenarios have been assessed, focusing on cooperative and controlled targets. Preliminary results show compliance with the capture condition and flexibility in terms of concept of operations. The proposed architecture can be further expanded to account for non-nominal scenarios, such as collision avoidance maneuvers, with minor modifications required.

1 INTRODUCTION

In-Orbit Logistics (IOL) is becoming one of the fastest growing markets within the European space ecosystem. According to ESA CM22, Europe shall be able to provide transportation services to- and in-space by 2030, including in-orbit servicing, in-space manufacturing and assembly, end-of-life management, Active Debris Removal (ADR), re-entry, etc. In order to reach this vision and acquire the relevant transport capabilities, two In-Space Transportation Proof-of-Concept (PoC) missions are planned to be implemented by ESA and the European space industry [1].

To give a response to the growth of the IOL market and participate in ESA IOL ecosystem, SENER has been developing solutions focused on standard interfaces for docking on the one side and GNC on the other. Regarding the first, the SENER docking and refuelling interface, SIROM, is an already mature product under qualification and envisioned for in-orbit demonstration missions such as EROSS or PoC-1 [2]. On the GNC side, the company has been developing architectures and algorithms compatible with cooperative and uncooperative rendezvous scenarios, applying the internal technologies on optimization-based guidance and control, as well as optical navigation schemes. Given such expertise, SENER has participated in several consortia in the Phase O/A of the first Proof-of-Concept mission, PoC-1. In particular, SIROM is being baselined for the following consortia at this early point: Thales Alenia Space (TAS), OHB SE and The Exploration Company (TEC). On the other hand, SENER is responsible for the optimization-based GNC for the OHB SE

and TEC consortia. The main objective of PoC-1 is the preliminary technological development of mechanical and electrical coupling interfaces, communication interfaces and autonomous rendezvous and docking GNC between cooperative vehicles.

This paper focuses on the developments that SENER has performed for rendezvous and docking GNC within the frame of PoC-1 and previous internal activities. The GNC is designed, sized, and simulated considering overall system performances and operations, as well as ensuring compatibility with the SIROM capture requirements, to guarantee the feasibility of the mating scenario. Furthermore, the design aims at providing operational flexibility in terms of approach direction, waypoints definition, trajectory/attitude constraints, etc. This is achieved by mains of an optimization-based guidance and control strategy, together with a cooperative relative navigation architecture.

The structure of the paper is as follows:

- Section 2 is dedicated to the description of the GNC architecture for cooperative rendezvous and docking, presenting the guidance and control scheme envisioned for the trajectory and attitude problems, together with the cooperative relative navigation architecture for the different phases of the maneuver.
- Section 3 focuses on the optimization-based guidance and control strategy, including the formulation of the optimal control problem and some notes on its implementation in a Model Predictive Control (MPC) architecture.
- Section 4 is devoted to the description of the cooperative navigation strategy, including marker-based relative navigation for the final approach and docking.
- Section 5 is the GNC performance results, obtained from the closed-loop simulation of the envisioned architecture and algorithms for a different set of maneuvers.
- Section 6 contains the conclusions of the presented work.

2 GNC ARCHITECTURE FOR COOPERATIVE RENDEZVOUS AND DOCKING

This section introduces the GNC architecture for cooperative rendezvous and docking. The GNC is designed and sized to comply with SIROM capture requirements, which are mainly summarized by a capture envelope in attitude, position, and time. The GNC needs to be able to maintain the docking interfaces within the capture envelope during a 1 second capture time for the capture to be successful. The size of the capture envelope depends on the spacecraft inertia properties and rotational stiffness. According to SENER analyses, for angular misalignments in the order of 0.5 degrees and vehicle masses in the order of 200 kg, the capture envelope is a cube of 10 mm side length, as shown in Table 1.

Table 1. SIROM capture envelope for low angular misalignments and vehicle masses in the order of 200 kg

$\delta\theta_x$ [deg]	$\delta\theta_y$ [deg]	$\delta\theta_z$ [deg]	δx [mm]	δy [mm]	δz [mm]
0.5	0.5	0.5	10.0	10.0	10.0

Next paragraphs describe the envisioned architecture for the different GNC functions. The position and attitude guidance and control formulations are decoupled. The guidance and control functions for the position are merged in an MPC scheme, for which the Optimal Control Problem (OCP) is formulated as a convex one, ensuring convergence guarantees and enabling real time computation. The attitude problem, on the other hand, is addressed by targeting a fixed relative attitude between both spacecraft and controlling it by means of a Proportional-Derivative (PD) controller. An

alternative currently under study is the use of Sequential Convex Programming (SCP) schemes for addressing the non-linearity of the attitude problem and working with an MPC on that side of the problem as well. It is relevant to mention that the main objective of the architecture at this point is the final approach and docking phases, in which the assumption of constant relative attitude is valid, in order to ease the mechanical capture and the optical instruments visibility of the client. SENER has already implemented and tested optimization-based algorithms for the attitude guidance and control problem in rendezvous scenarios, with Line-of-Sight (LoS) constraints [3][4]. Further developments of PoC-1 GNC architecture may also include this attitude guidance and control strategy. To close the guidance and control pipeline, the control allocation problem is also formulated as convex optimization problem, as it will be further developed in Section 3.

Regarding the navigation function, a distinction is to be made between absolute and relative navigation architectures. The later depends on the servicer-client range, in order to account for the relative navigation sensors employed along the different phases of the approach. Those are: Wide-Angle Cameras (WAC), Narrow-Angle Cameras (NAC) and Laser Rangefinder (LRF). Since the envisioned relative navigation architecture is cooperative, the client is equipped with visual fiducial markers for pose reconstruction during the final approach, and the client navigation message will be employed in the estimation of the relative state. Such navigation message contains the client absolute navigation solution, together with housekeeping and mass variables, among others, and is transmitted to the servicer via Inter-Satellite Link (ISL).

Concerning the initial and intermediate approach, in which the client markers cannot be identified, the relative position estimation is based on the absolute position solution computed by each spacecraft and is aided by NAC measurements, for higher robustness and in order to reduce the performance degradation due to transmission delays. Centre of Brightness or bearings-only navigation techniques can be employed to obtain the relative position solution from the NAC measurements. The relative velocity and rotational state estimation is primarily based on the combination of both absolute state solutions.

During the last meters of the approach, as the markers become identifiable, the relative position estimation relies mainly on the information from the camera for the in-plane relative position and the laser rangefinder for the range. On the other hand, the relative velocity is mainly obtained by fusing the absolute velocity solutions of each spacecraft. The absolute navigation solution of both spacecraft is also the main source for the estimation of the relative rotational state, due to the fact that marker-based attitude estimation performance is not enough to meet typical capture requirements, as shown in Section 4. Such absolute attitude solution is considered to be obtained by data fusion of the star tracker and inertial measurements onboard each spacecraft.

3 OPTIMIZATION-BASED GUIDANCE AND CONTROL IMPLEMENTATION

This section presents the guidance and control implementation, putting special attention to the mathematical formulation of the OCP and providing some overview of the solution strategy. As it was mentioned in Section 2, the guidance and control function is based on optimization and includes the solution of the control allocation problem. For the latter, the use of Chemical Propulsion (CP) is the baseline for this architecture both for attitude and position control, but it can accommodate Electric Propulsion (EP), a combination of CP and EP, or other devices simultaneously such as reaction wheels, with minor changes required. The guidance and control problem is addressed by decoupling the relative translation, the servicer attitude optimization problems, and the optimal control allocation, as shown in Fig. 1. The output of the optimal thrust dispatching is the thrust level for each thruster, which is fed to a Pulse Width Modulator (PWM), transforming the thrust profile to actuation pulses. It is relevant to remark at this point that the PWM was designed to accumulate pulses

with duration below the minimum on-time, which is directly related to the Minimum Impulse Bit (MIB). This allows certain anticipation capabilities that result in a performance improvement, especially for thrusters with high MIB.

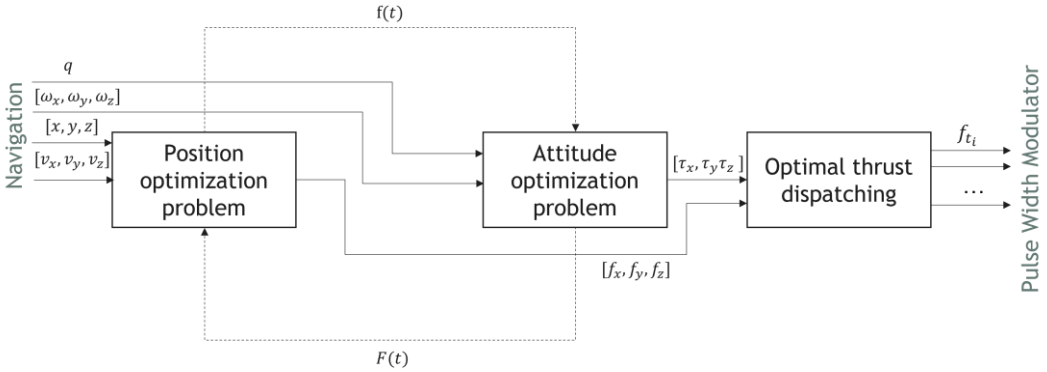

Figure 1. Optimization-based guidance and control architecture

The relative translation guidance and control problem is formulated in Hill's frame. As shown in Fig. 2, this frame is centred on the client spacecraft centre of mass and defined with the $\hat{\imath}$-direction pointing radially outwards from the Earth, the $\hat{\jmath}$-direction along the client's in-track —i.e., the client's velocity vector direction—, and the $\hat{k}$-direction aligned with the angular momentum direction, completing the triad. The unit vectors associated to this frame are sometimes also defined as R-bar, V-bar, and H-bar.

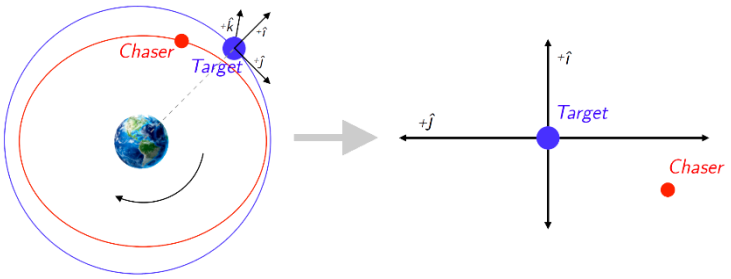

Figure 2. Hill's reference frame definition

The convex formulation of the of the relative translation problem is possible thanks to the use of the Hill-Clohessy-Wiltshire (HCW) equations, depicted in Eq. 1, which are a linearized dynamic model. The premise of its establishment is the relative distance between the two spacecraft being much less than the client's orbital radius and the client moving in a low eccentricity orbit and with a first-order approximation of the gravitational field [5]. Such convex formulation allows solving the position OCP by means of the in-house Interior Point Method solvers reliably and efficiently [3][6].

$$\begin{cases} \ddot{x} - 2n\dot{y} - 3n^2 x = f_x/m \\ \ddot{y} + 2n\dot{x} = f_y/m \\ \ddot{z} + n^2 z = f_z/m \end{cases} \tag{1}$$

External differential perturbations are neglected in the formulation and resolution of the optimal guidance problem and are captured by the closed-loop control feedback instead. This decision enhances the real-time reliability of the problem but is also reasonable, mainly due to the fact that differential perturbations are small as compared to gravity and control forces. Taking this assumption into account, the vector of external forces corresponds to the control force. Therefore, the system in

Eq. 1 can be written in a Linear Time-Invariant (LTI) state-space form as $\dot{\bar{x}} = A\bar{x} + B\bar{u} = f(\bar{x}, \bar{u}, n, m)$, where $\bar{x} = [x, y, z, \dot{x}, \dot{y}, \dot{z}]^T$, $\bar{u} = [f_x, f_y, f_z]^T$ and the state and control matrices given by Eq. 2.

$$A = \begin{bmatrix} 0 & 0 & 0 & 1 & 0 & 0 \\ 0 & 0 & 0 & 0 & 1 & 0 \\ 0 & 0 & 0 & 0 & 0 & 1 \\ 3n^2 & 0 & 0 & 0 & 2n & 0 \\ 0 & 0 & 0 & -2n & 0 & 0 \\ 0 & 0 & -n^2 & 0 & 0 & 0 \end{bmatrix} \qquad B = \begin{bmatrix} 0 & 0 & 0 \\ 0 & 0 & 0 \\ 0 & 0 & 0 \\ 1 & 0 & 0 \\ 0 & 1 & 0 \\ 0 & 0 & 1 \end{bmatrix} \tag{2}$$

From Eq. 1 one can see that the relative motions inside and outside the orbital plane are decoupled when described by the HCW equations. Looking at the relative motion inside the orbital plane, it can be proven that the system natural path —i.e., when $\bar{u} = \bar{0}$— is an ellipse defined by Eq. 3. For the particular case in which $x_0 = \dot{x}_0 = \dot{y}_0 = 0$ and $y_0 \neq 0$, the initial in-plane state (x_0, y_0) is a stable system node [7].

$$\frac{(x - a_1 + 3a_2 nt)^2}{(2a_3)^2} + \frac{(z - 2a_2)^2}{(a_3)^2} = 1 \qquad a_1 = y_0 - \frac{2\dot{x}_0}{n} \qquad a_2 = 2x_0 + \frac{\dot{y}_0}{n} \qquad a_3 = \left[\left(\frac{2\dot{y}_0}{n} + 3x_0\right)^2 + \left(\frac{\dot{x}_0}{n}\right)^2\right]^{1/2} \tag{3}$$

Since the problem is linear, an exact analytical form for $x_{i+1} = f_i(x_i, u_i) = A_d x_i + B_d u_i$ exists. Defining T as the discretization time-step, the discrete state transition matrices can be expressed as in Eq. 4. The problem is convex and is divided into two sub-problems: the intermediate approach problem, aimed at tracking a given reference with approach corridor constraints, and the final approach and docking problem, aimed at tracking the docking port state.

$$A_d = \begin{bmatrix} 4 - 3\cos nT & 0 & 0 & \frac{1}{n}\sin nT & \frac{2}{n}(1 - \cos nT) & 0 \\ 6(\sin nT - nT) & 1 & 0 & \frac{-2}{n}(1 - \cos nT) & \frac{1}{n}(4\sin nT - 3nT) & 0 \\ 0 & 0 & \cos nT & 0 & 0 & \frac{1}{n}\sin nT \\ 3n\cos nT & 0 & 0 & \cos nT & 2\sin nT & 0 \\ -6n(1 - \cos nT) & 0 & 0 & -2\sin nT & 4\cos nT - 3 & 0 \\ 0 & 0 & -n\sin nT & 0 & 0 & \cos nT \end{bmatrix}$$

$$B_d = \begin{bmatrix} \frac{1}{n^2}(1 - \cos nT) & \frac{2}{n^2}(nT - \sin nT) & 0 \\ \frac{-2}{n^2}(nT - \sin nT) & \frac{4}{n^2}(1 - \cos nT) - \frac{3}{2}T^2 & 0 \\ 0 & 0 & \frac{1}{n^2}(1 - \cos nT) \\ \frac{1}{n}\sin nT & \frac{2}{n}(1 - \cos nT) & 0 \\ \frac{-2}{n}(1 - \cos nT) & \frac{4}{n}\sin nT - 3T & 0 \\ 0 & 0 & \frac{1}{n}\sin nT \end{bmatrix} \tag{4}$$

The formulation of the relative translational state optimization problem for the intermediate approach is shown in Eq. 5. The problem is implemented in a receding horizon fashion and is intended to provide translational state reference tracking. The dynamic model is the discretised HCW equations, as per Eq. 4. The objective function contains the minimization of the state tracking error and the propellant consumption. In terms of the problem constraints, the force is restricted with a polytope, considering the spacecraft attitude and thruster configuration. This ensures that the obtained

commands lie within the actuation envelope. Furthermore, the relative position is restricted to be contained within the approach corridor. As it is shown in the formulation of the problem, this constraint is relaxed by means of a single slack variable, using an l_∞ term added to the cost function. The approach corridor constraint is approximated as a pyramidal one to reduce the computational load. An additional plane can be used at a given distance from the client to ensure the safety in the tracking of the last waypoint prior to docking.

$$\begin{aligned} &\min_{x_i,F_i,\gamma} \left(x_N - x_{ref_N}\right)^T P\left(x_N - x_{ref_N}\right) + \omega\gamma + \sum_{i=0}^{N-1} \frac{1}{2}\left(x_i - x_{ref_i}\right)^T L_i\left(x_i - x_{ref_i}\right) + \frac{1}{2} F_i^T R_i F_i \\ &s.t. \quad x_{i+1} = A_{HCW} x_i + B_{HCW} F_i \\ &\qquad A_i^u F_i \leq b_i^u \\ &\qquad A^x x_i \leq b^x + \gamma \\ &\qquad \gamma \geq 0 \\ &\qquad x_0 = \overline{x_0} \end{aligned} \tag{5}$$

As for the relative translational state optimization problem for the final approach and docking, its mathematical formulation is shown in Eq. 6. This problem is implemented in a shrinking horizon scheme, updated with the predicted docking time. Its objective is tracking the docking port state. The dynamic model is the discretised HCW equations, as per Eq. 4. For this case, no constraints on the state are included. Instead, the optimal trajectory is encouraged to follow a straight line in the middle of the approach corridor by suitable cost tuning. Note that the decision of approaching in a straight line simplifies the optical instruments pointing in the final approach, as well as the mechanical capture. The force, on the other hand, is still restricted with a polytope, considering the spacecraft attitude.

$$\begin{aligned} &\min_{x_i,F_i,\gamma} \left(x_N - x_{ref_N}\right)^T P\left(x_N - x_{ref_N}\right) + \omega\gamma + \sum_{i=0}^{N-1} \frac{1}{2}\left(x_i - x_{ref_i}\right)^T L_i\left(x_i - x_{ref_i}\right) + \frac{1}{2} F_i^T R_i F_i \\ &s.t. \quad x_{i+1} = A_{HCW} x_i + B_{HCW} F_i \\ &\qquad A_i^u F_i \leq b_i^u \\ &\qquad x_0 = \overline{x_0} \end{aligned} \tag{6}$$

The attitude guidance strategy as of today is addressed by targeting a fixed relative angular state between both spacecraft, being the relative attitude currently controlled by means of a PD controller. This attitude targeting simplifies the decoupling between the problems, assigning the control allocation with managing unfeasible simultaneous torque and force commands. Nonetheless, based on previous optimization-based implementations by SENER of the attitude guidance and control problem for rendezvous, the PD-based attitude control scheme will be revisited and formulated as described next [3][4].

Consider the LoS management problem defined in Fig. 3, where $\bar{r}$ represents the servicer-client direction expressed in the inertial frame and $\bar{v}$ is the optical sensor boresight axis in the spacecraft body frame. The angles θ_{imax} and θ_{vmax} represent the Field of View (FoV) of two arbitrary optical sensors and θ_{sun} is the minimum angle between the boresight axis and the sun pointing vector for instrument blinding avoidance [8]. Defining θ as the instantaneous angle between the optical sensor and the client direction, it is trivial to derive $\cos\theta = \bar{r} \cdot \bar{v}$. Notice that $\bar{v}$ is a constant vector in the servicer body frame, while $\bar{r}$ can be obtained from the relative navigation function. The rotation axis between $\bar{r}$ and $\bar{v}$ is $\hat{e} = \bar{r} \times \bar{v} / |\bar{r} \times \bar{v}|$. These two relations allow computing the rotation quaternion between the pointing objective direction and the instantaneous instrument axis in inertial frame as $\bar{q}_{rv} = [\hat{e}\sin(\theta/2), \cos(\theta/2)]$. Therefore, at any time instant *k*, the reference spacecraft attitude quaternion for LoS tracking is $\bar{q}_k = \bar{q}_{k-1} \otimes \bar{q}_{rv}$. The q_4 quaternion convention is used here and will be maintained along the whole document, meaning that the scalar part is the fourth element of the quaternion.

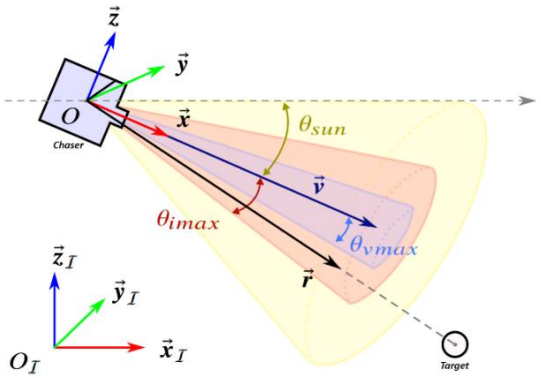

Figure 3. LoS management problem definition (adapted from [8])

The governing equations for the servicer spacecraft rotational state are given by Eq. 7 [9], where $\bar{q}_{bi}$ and $\bar{\omega}_{bi}$ are the servicer attitude quaternion and angular velocity vector with respect to the inertial frame, respectively, $\bar{\bar{J}}_b$ is the servicer inertia tensor in body frame and $\bar{L}_b$ is the torque vector in body frame, which will be the control degree of freedom in the optimization problem. This torque is assumed to be generated by an actuation device presenting no residual torque at the beginning of the maneuver. External environmental perturbations to the rotational state are not included in the formulation of the optimization problem.

$$\begin{cases} \dot{\bar{q}}_{bi} = \frac{1}{2}\bar{\omega}_{bi} \otimes \bar{q}_{bi} \\ \dot{\bar{\omega}}_{bi} = \bar{\bar{J}}_b^{-1}\left[\bar{L}_b - \bar{\omega}_{bi} \times \left(\bar{\bar{J}}_b \bar{\omega}_{bi}\right)\right] \end{cases} \tag{7}$$

The servicer LoS tracking optimization problem is formulated as in Eq. 8. The objective function is defined so that the combination of the servicer attitude quaternion with respect to the reference quaternion and the control effort is minimised along the whole path, hence a path tracking problem. Since the problem is non-linear, the continuous dynamics $\dot{x} = g(x,u) = [\dot{\bar{q}}_{bi}, \dot{\bar{\omega}}_{bi}]$ (Eq. 7) and their Jacobians $A = \partial g(x,u)/\partial x$ and $B = \partial g(x,u)/\partial u$ are used. The control vector is limited to the maximum available torque and the attitude quaternion is constrained by the optical instruments FoV, so that the client remains visible during the whole maneuver. This constraint may be softened in the future by means of slack variables to increase robustness. In the attitude optimization problem, a good initial guess for the SCP can be obtained from the tracking reference, computed from the first position optimization problem. This can potentially reduce the number of SCP iterations to one.

$$\begin{aligned} &\min_{x_i, F_i, \gamma} \left(x_N^q - x_{ref_N}^q\right)^T P\left(x_N^q - x_{ref_N}^q\right) + \omega\gamma + \sum_{i=0}^{N-1} \frac{1}{2}\left(x_i^q - x_{ref_i}^q\right)^T L_i \left(x_i^q - x_{ref_i}^q\right) + \frac{1}{2} F_i^T R_i F_i \\ &s.t. \quad x_{i+1} = Ax_i + BT_i \\ &\qquad |u_i| \le T_{max} \\ &\qquad \bar{q}^T (I - P(\bar{r}, \bar{v})\bar{q} \le 1 + \cos\theta_{min} \\ &\qquad \bar{q}^T (I - P(\bar{r}, \bar{v})\bar{q} \le 1 - \cos\theta_{max} \\ &\qquad x_0 = \overline{x_0} \end{aligned} \tag{8}$$

where,

$$P(\bar{r}, \bar{v}) \equiv \begin{bmatrix} [\bar{r}]^\times & \bar{r} \\ -\bar{r}^T & o \end{bmatrix} \begin{bmatrix} -[\bar{v}]^\times & \bar{v} \\ -\bar{v}^T & o \end{bmatrix}$$

Finally, the guidance and control function includes the resolution of the optimal control allocation problem. Its mathematical formulation is shown in Eq. 9. The thrust direction matrix is given by $A_{F,k} = [\bar{v}_k]$, while the torque direction matrix is $A_{\tau,k} = [\bar{r}_k \times \bar{v}_k]$, where $\bar{v}_k$ is the thrust direction of thrusters k in body frame and $\bar{r}_k$ is the position vector of thruster k in body frame. The matrix A_{Fd} can

be defined as $A_{Fd,ij} = \bar{n}_i \cdot \bar{v}_j \, , i = 1{,}2 \, , j = 1{:}\, n_{\text{thrusters}}$, with $\bar{n}_i, \bar{v}_j \in \mathbb{R}^3$, $|\bar{n}_i| = |\bar{v}_j| = 1$ and the $\bar{n}_i$ vectors being perpendicular among themselves and representing the two orthogonal directions with respect to the desired command one. This constraint ensures that the executed force lies in the same direction as the commanded. Therefore, force error is allowed in order to relax the problem in the case of an unfeasible combination of torque and error commands, but the overall Δv is executed along the desired path.

$$\begin{aligned} \min_{f_i} \quad & 1^T f_i + \frac{1}{2}(F - A_F f_i)^T Q (F - A_F f_i) \\ s.t. \quad & 0 \le f_i \le f_{max} \\ & A_\tau f \;\; = T \\ & A_{Fd} f = 0 \end{aligned} \tag{9}$$

The maximum force level is constrained to the equivalent of a maximum pulse, given the PWM frequency, while the MIB is assumed to be zero at optimization level to avoid either having a non-convex constraint of the type $f_i \in 0 \cup [f_{MIB}, f_{max}]$ or all thrusters simultaneously firing as per $f_i \in [f_{MIB}, f_{max}]$. This constraint could eventually be changed to include the MIB or allow for differential thrusting. Nonetheless, at this point of the development, the PWM is configured to accumulate any pulse below the MIB commanded by the control function. Together with the constraint on the force direction, a hard constraint forcing a zero torque error is included. The later may be relaxed in the future, increasing the robustness of the formulation. The objective function is formulated for propellant and force error minimization, using a combination of linear and quadratic terms. As a final remark, it is worth pointing out that the solution of the optimization problems involved in the GNC and presented before is enabled by the in-house autocodable optimization toolbox, the SENER Optimization Toolbox (SOTB).

4 MARKER-BASED RELATIVE NAVIGATION IMPLEMENTATION

This section focuses on the relative navigation scheme implementation for the final approach and docking. As introduced in Section 2, during this phase, the client markers are identifiable and therefore, the data fusion architecture contains the measurements of the camera, the laser rangefinder, and the absolute navigation solution of both spacecraft.

ArUco fiducial markers are used, together a visual-spectrum WAC, for the identification of the client. The main advantage of ArUco markers is the fact that they are a standard in the robotics field and have been previously flown. Consequently, there is extensive state-of-the-art in terms of processing algorithms and even built-in libraries like OpenCV. On the other hand, due to the fact that ArUco markers can only be identified in the visible light spectrum, their usage poses non-negligible constraints in the illumination conditions during the final approach and docking maneuver, which may drive the selection of the orbit and limit the flexibility of the CONOPs. For the preliminary design of the GNC in the frame of PoC-1, ArUco markers were baselined, as their performance can be easily characterised and included in the GNC loop. Nonetheless, further iterations of the design will include the assessment of the performance of additional client identification systems, such as visual-infrared markers, like the Marker Support Navigation (MSN) by Admatis [10]. This will aim at relaxing the constraints on the mission in terms of illumination conditions. Fig. 4 shows a graphical representation of ArUco and MSN 2D and 3D markers, for a qualitative comparison.

First of all, and in order to characterize the pose estimation performance when processing ArUco markers images, a sensitivity analysis was carried out on the camera and marker parameters and the marker configuration. Next, a Monte Carlo analysis for the selected configuration was executed,

aimed at extracting the marker-based relative navigation performances, as a function of the relative range and for variable angular misalignments between both spacecraft.

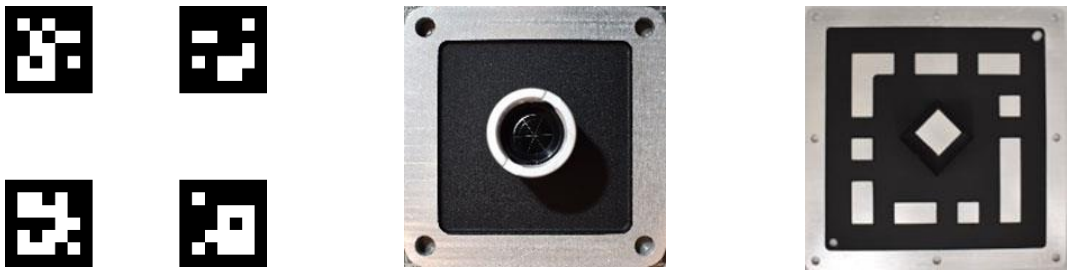

Figure 4. ArUco markers (left), MSN 2D markers (centre), MSN 3D markers (right)

The sensitivity analysis was intended to identify the most favourable configuration in terms of camera and marker characteristics and marker configuration. Hence, the following parameters were varied: marker length, camera FoV and number of pixels, marker separation and number of markers per face. The navigation performance figures of merit are the knowledge error in the out-of-plane rotations, $\delta\hat{\theta}_x$ and $\delta\hat{\theta}_y$, the rotation around the boresight axis, $\delta\hat{\theta}_z$, the translation errors in the lens plane, $\delta\hat{x}$ and $\delta\hat{y}$, and the out-of-plane translation error, $\delta\hat{z}$. Table 2 shows the reference case in terms of camera and marker configuration. Comparing the state knowledge error with the results in the reference case, Table 3 shows a summary of the relative navigation performance sensitivities with respect to the reference case. Two representative distances are chosen for the analysis: one close to marker acquisition (around 10 meters) and another one close to docking (around 1 meter).

Looking at the results obtained, it is concluded that reducing the number of markers with respect to the reference case severely hinders the estimation performance. An analogous conclusion is drawn when reducing the lens pixel size. On the other hand, increasing the marker separation improves the relative rotation estimation in the far range, but increases further the close-range position estimation error. Increasing the camera FoV decreases the navigation performance in general. Furthermore, it reduces the distance range for marker identification, which is an additional detrimental effect. Finally, increasing the marker length benefits the relative rotation estimation, but decreases the relative position estimation accuracy. While it also increases the distance range at which the markers are identifiable, it may lead to docking requirements non-compliance in terms of in-plane relative position knowledge, which are the most relevant components to be estimated using the marker-based relative navigation.

Table 2: Marker-based relative navigation reference case

Field of View [deg]	Number of pixels [-]	Marker length [cm]	Marker separation [cm]	Number of markers per face [-]	Marker layout
35	2048 x 2048	6.0	15.0	4	2 x 2

Table 3: Sensitivity analysis to camera and marker configuration with respect to the reference case

Sensitivity case	Distance [m]	$\delta\hat{\theta}_x$ [%]	$\delta\hat{\theta}_y$ [%]	$\delta\hat{\theta}_z$ [%]	$\delta\hat{x}$ [%]	$\delta\hat{y}$ [%]	$\delta\hat{z}$ [%]
Marker length +150%	1	-30.0	+0.0	-46.2	+25.0	+25.0	+85.7
	10	-25.0	-27.3	-25.0	+22.7	+35.0	-16.7
Camera FoV +130%	1	+70.0	+77.8	-23.8	+25.0	+25.0	-28.6
	10	+16.7	+2.7	+65.0	+36.4	+50.0	-25.0
Camera number of pixels -50%	1	+150.0	+122.2	+53.9	+100.0	+125.0	+42.9
	10	+66.7	+54.6	+400.0	+172.7	+250.0	+100.0

Marker separation +350%	1	+50.0	+33.3	-46.2	+175.0	+300.0	+128.6
	10	-30.0	-27.3	-40.0	+40.9	+50.0	-25.0
2 markers (horizontal configuration)	1	+590.0	+388.9	+100.0	+150.0	+150.0	+92.9
	10	+250.0	-79.1	+30.0	+4.6	+85.0	-25.0
2 markers (vertical configuration)	1	+350.0	+677.8	+207.7	+100.0	+100.0	+71.4
	10	-77.5	+309.1	+300.0	+68.2	+0.0	-8.3
2 markers (diagonal configuration)	1	+710.0	+722.2	+207.7	+200.0	+225.0	+185.7
	10	+208.3	+254.6	+800.0	-13.6	-15.0	-33.3
1 marker (centred configuration)	1	+240.0	+344.4	+53.9	+300.0	+250.0	+0.0
	10	+66.7	+54.6	+300.0	+627.3	+550.0	+400.0

Based on this sensitivity analysis, it is concluded that the selected configuration for the marker-based relative navigation corresponds to the reference case shown in Table 2. For such configuration, a Monte Carlo campaign was executed, perturbing the angular misalignment between both spacecraft and parametrizing the range between them. The relative state knowledge error as a function of the range is shown in Fig 5. The grey points are the Monte Carlo simulated cases, while black and blue lines are the interpolated mean and 3σ envelopes, respectively. The first thing that becomes apparent is the increase in the relative state knowledge error with range. In terms of attitude knowledge error, the out-of-plane rotations follow a similar trend, and their error is in the order of degrees. On the other hand, the rotation error along the boresight axis presents a two orders of magnitude lower estimation error and is in the order of 0.1 degrees. As for the relative translational state, the knowledge along the camera plane is in the order of millimetres, while the position estimation error along the boresight axis is two orders of magnitude higher.

Finally, Table 4 shows a summary of the obtained marker-based relative navigation performance, expressed as 3σ quantities. The in-plane relative position knowledge is enough to satisfy the GNC requirements for docking, while additional measurements are required to increase the knowledge of the relative attitude and range. As introduced in Section 2, the camera measurements will be fused with the laser rangefinder measurements for increased range knowledge, and with the absolute rotational state solution of both spacecraft, for increased attitude knowledge.

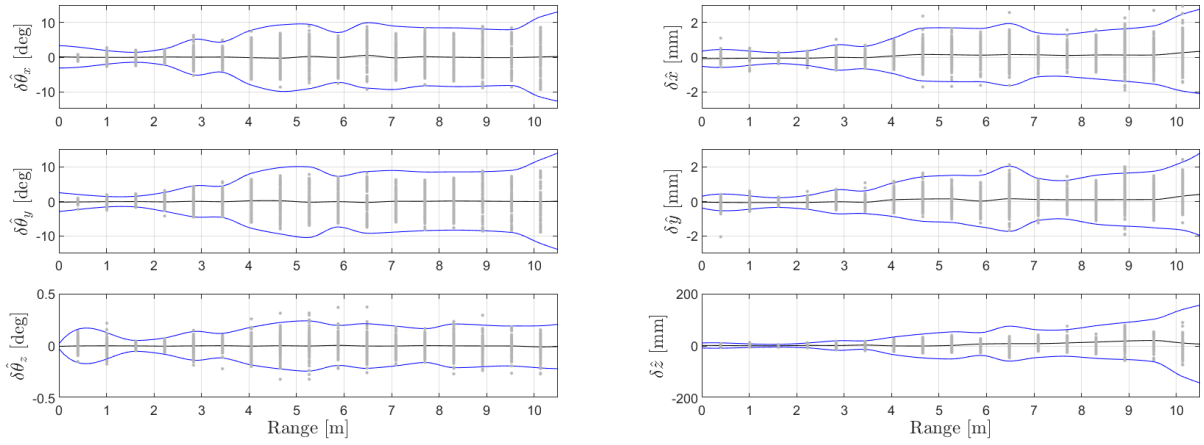

Figure 5. Marker-based relative state knowledge error as a function of range

Table 4: Marker-based relative navigation performance

Distance [m]	$\delta\hat{\theta}_x$ **[deg]**	$\delta\hat{\theta}_y$ **[deg]**	$\delta\hat{\theta}_z$ **[deg]**	$\delta\hat{x}$ **[mm]**	$\delta\hat{y}$ **[mm]**	$\delta\hat{z}$ **[mm]**
1	1.00	0.90	0.13	0.40	0.40	70.00
10	12.00	11.00	0.20	2.20	2.20	120.00

Considering the relative navigation architecture introduced in Section 2 and the obtained marker-based performance, the relative state knowledge budget can be computed, with special focus on the final approach and docking phases. The main contributions to the knowledge budget are listed next. For the relative position knowledge in the perpendicular plane to the docking axis, the main driver is the in-plane knowledge from the camera images processing. On the other hand, the range knowledge is conditioned by both the camera out-of-plane knowledge and the LRF measurements. As for the relative velocity knowledge, it is driven by the INS-GNSS performance and the inter-satellite link delay. Finally, for the relative attitude, the error contributions come mainly from the star tracker and gyroscope measurement error, together with the error due to the inter-satellite link delay. The relative angular velocity knowledge level is conditioned by the gyroscope measurement error and the inter-satellite link delay. Taking these contributions into account and considering a characteristic distance of one meter for the docking phase, the relative state knowledge budget, expressed as 3σ quantities is given by Table 5.

Table 5: Relative state knowledge budget for docking

$\delta\hat{\theta}_x$ (roll) [arcsec]	$\delta\hat{\theta}_y$ (pitch) [arcsec]	$\delta\hat{\theta}_z$ (yaw) [arcsec]	$\delta\hat{x}$ (V-bar) [mm]	$\delta\hat{y}$ (R-bar) [mm]	$\delta\hat{z}$ (H-bar) [mm]
90	90	90	3.0	2.0	2.0
$\delta\hat{\omega}_x$ (roll) [arcsec /s]	$\delta\hat{\omega}_y$ (pitch) [arcsec /s]	$\delta\hat{\omega}_z$ (yaw) [arcsec /s]	$\delta\hat{v}_x$ (V-bar) [mm/s]	$\delta\hat{v}_y$ (R-bar) [mm/s]	$\delta\hat{v}_x$ (H-bar) [mm/s]
51	51	51	2.8	2.8	2.8

With the proposed architecture, the relative navigation knowledge level was checked to be the main driver for the overall GNC performance. On top of that, the most demanding requirements coming from the mechanical interface are set on the relative translational state. Hence, it was deemed necessary to develop a custom relative data fusion scheme for the estimation of the relative position vector. This filter is intended to combine the camera and the laser rangefinder measurements. Future developments of the prototype will include the estimation of the complete relative state vector, including the information transmitted through inter-satellite link.

In terms of data fusion schemes, an Extended Kalman Filter was chosen for the prototype, given the non-linearity in the LRF measurement equation. Its formulation is described in next paragraphs. Consider the state vector given by $x = [x_{\mathrm{HCW}}, \dot{x}_{\mathrm{HCW}}]^T$, where x_{HCW} and $\dot{x}_{\mathrm{HCW}}$ are the relative position and velocity vectors in Hill's frame, respectively. The state propagation model is $\hat{x}_k^- = f(\hat{x}_{k-1}^+, u_k)$, where f is given by Eq. 10, and A_{HCW} and B_{HCW} are as in Eq. 4. The state transition matrix F_{k} is computed as per Eq. 11. Knowing the process noise Q_k allows propagating the state covariance matrix, P_k^-, as given by Eq. 12 [11].

$$\hat{x}_k^- = A_{\mathrm{HCW}}[\hat{x}_{\mathrm{HCW}}, \hat{\dot{x}}_{\mathrm{HCW}}]^T + B_{\mathrm{HCW}} u_{\mathrm{HCW}} \tag{10}$$

$$F_k = \frac{\partial f}{\partial x}\Big|_{\hat{x}_{k-1}^+} = A_{\mathrm{HCW}} \tag{11}$$

$$P_k^- = F_k P_{k-1}^+ F_k^T + Q_k \tag{12}$$

Given the rendezvous camera processed measurement equation $h_{\mathrm{RVC}} = x_{\mathrm{HCW}}$ and the laser rangefinder range measurement given by $h_{\mathrm{LRF}} = \rho_{\mathrm{HCW}} = |x_{\mathrm{HCW}}|$, the measurement innovation is computed as $y_k = z_k - h(\hat{x}_k^-)$, where z_k is the sensor measurement. These measurements allow updating the a-priori state propagation as $\hat{x}_k^+ = \hat{x}_k^- + K_k y_k$. The Kalman gain, K_k, is given by Eq. 13, where R_k is the measurement noise and H_k are the measurement matrices, shown in Eq. 14. A typical value for the measurement acquisition frequency in rendezvous cameras is 1 Hz, while LRF frequencies range between 20-50 Hz. Consequently, the envisioned measurement update strategy is

sequential, meaning that whenever a new LRF measurement is available, the previous state estimation is updated with it. On the other hand, whenever both the RVC and the LRF measurements are available, they update the state estimate one after the other. Sequential architectures allow reducing the computational load of the data fusion scheme, as well as making the algorithm flexible to a wide range of measurement inputs and asynchronous or synchronous frequencies. The complete data fusion strategy is shown in Algorithm 1.

$$K_k = P_k^- H_k^T (H_k P_k^- H_k^T + R_k)^{-1} \tag{13}$$

$$H_{k,\mathrm{RVC}} = \left.\frac{\partial h_{\mathrm{RVC}}}{\partial x}\right|_{\hat{x}_k^-} = I_{3,3} \qquad H_{k,\mathrm{LRF}} = \left.\frac{\partial h_{\mathrm{LRF}}}{\partial x}\right|_{\hat{x}_k^-} = \begin{bmatrix} \frac{x_{\mathrm{HCW,x}}}{|x_{\mathrm{HCW}}|} & 0 & 0 \\ 0 & \frac{x_{\mathrm{HCW,y}}}{|x_{\mathrm{HCW}}|} & 0 \\ 0 & 0 & \frac{x_{\mathrm{HCW,z}}}{|x_{\mathrm{HCW}}|} \end{bmatrix} \tag{14}$$

Algorithm 1: Relative position Extended Kalman Filter

1. Propagate state: $\hat{x}_k^- \leftarrow f(\hat{x}_{k-1}^+, u_k)$
2. Propagate state covariance matrix: $P_k^- \leftarrow F_k P_{k-1}^+ F_k^T + Q_k$

Sequentially for the camera and laser rangefinder measurements:

3. Compute measurement innovation: $y_k \leftarrow z_k - h(\hat{x}_k^-)$
4. Compute Kalman gain: $K_k \leftarrow P_k^- H_k^T (H_k P_k^- H_k^T + R_k)^{-1}$
5. Update state estimate: $\hat{x}_k^+ \leftarrow \hat{x}_k^- + K_k y_k$

5 GNC PERFORMANCE RESULTS

This section presents the main results obtained after the simulation of the closed-loop GNC architecture and its implementation described in previous sections. In order to particularise the GNC design to a specific mission architecture and concept of operations, two maneuvers were considered: an approach along the V-bar and a combined VR-bar approach. Furthermore, intermediate holding points were also included in the maneuvers, simulating operational Go/No-Go points and the required stops to allow for the navigation filters convergence. This allows addressing the flexibility of the envisioned GNC concept not only to different approach directions, but also to various mission and operational constraints.

The closed-loop simulation infrastructure accounts for sensor and estimation errors, control and dispatching errors and environmental perturbations. The considered spacecraft main characteristics are shown in Table 6. The capture condition is given by SIROM requirements, shown in Table 1. In particular, the GNC shall be able to provide a 10x10x10 mm envelope during 1 second and with angular misalignments lower than 0.5 degrees. The GNC was tuned according to this capture criteria. Both dynamic transfers and holding points present an analogous guidance and control scheme, based on MPC. As for the holding points, and in order to prevent over-actuation, a configurable position deadband and stabilisation time are included, allowing the spacecraft to drift within a predefined sphere centred in the nominal waypoint.

Table 6. Spacecraft main characteristics for closed-loop GNC simulation

Parameter	Description	Value
MIB	Minimum Impulse Bit	0.025 Ns
oT_{max}	Maximum On Time	20 s
F_{nom}	Nominal thrust per actuator	1 N
M_{SC}	Spacecraft mass (assumed constant)	200 kg

The first maneuver type studied from a GNC perspective is the approach from the negative V-bar direction, with holding points at 1000-, 500- and 20-meters range. The analysis consists of a Monte Carlo campaign with perturbations in the initial relative position and velocity and a total of 100 runs. Fig. 6 shows the obtained trajectories. The initial perturbations in the out-of-plane (Z-bar) direction are quickly absorbed by the MPC scheme, leading to hopping-like dynamic segments in the R-/V-bar plane. The exception to this is the transfer from the 20 meters holding point to the capture envelope, which is intendedly executed along the V-bar axis, in order to ease the optical instruments pointing and the final capture during the last dynamic segment.

The capture condition is met in 100% of the Monte Carlo cases. In terms of ΔV maneuver cost, considering both dynamic segments and 1 hour holding points, the obtained $\mu + 3\sigma$ cost is 12.79 m/s. Even though, as mentioned before, a position deadband was included for the holding points, the main contribution to the ΔV budget comes from the static segments. This is reasonable considering their budgeted duration and can be tuned by means of the stabilisation time and position deadband parameters. Likewise, the cost of the transfer arcs can be traded-off with their duration, being this one of the advantages of the use of an MPC-based guidance and control strategy.

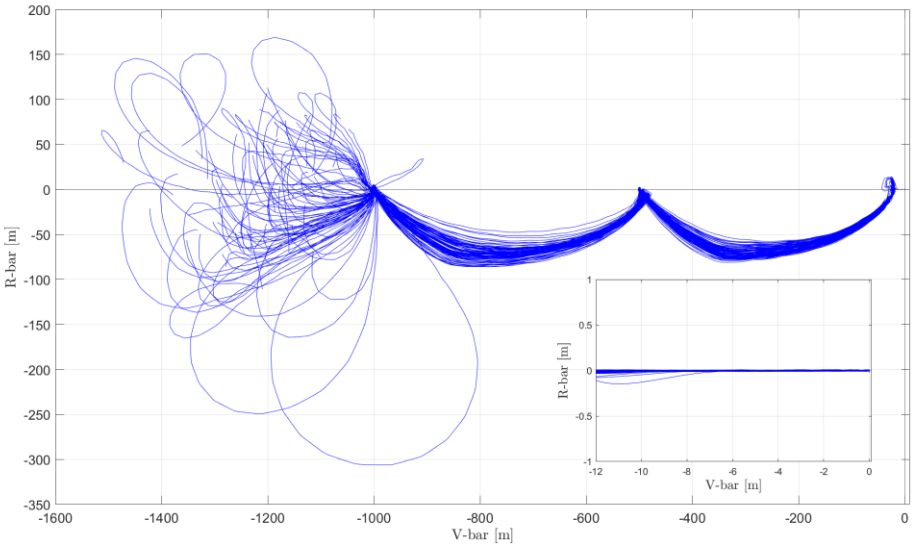

Figure 6. Relative position in Hill's frame for the V-bar approach

The second maneuver considered is a combined RV-bar approach. It is based on an initial approach along the negative V-bar up to 500 meters range, including holding points at 1000 and 500 meters. Then, a transfer arc is executed to a holding point at 200 meters range along the negative R-bar direction, to conclude the maneuver along such direction and including an additional holding point at 20 meters range. The analysis, as in the previous case, consists of a Monte Carlo campaign with perturbations in the initial relative position and velocity and a total of 100 runs. In order to reduce the effort in simulation, the results shown in this case correspond to the union of the corresponding segments along R- and V-bar, instead of simulations merging the complete operation. The obtained trajectories are shown in Fig. 7. As in the previous maneuver, the last dynamic segment is constrained to a straight line in this Hill's frame and, therefore, is executed along the negative R-bar direction for this second maneuver. The capture condition is met in 100% of the Monte Carlo cases. In terms of the maneuver ΔV, considering both dynamic segments and 1 hour holding points, the obtained $\mu + 3\sigma$ cost is 21.15 m/s.

The most important outcome from the GNC performance analysis is the success in achieving the required accuracy for capture in all the cases simulated with the still preliminary GNC design. The

flexibility of the architecture has also been demonstrated, which accommodates virtually any approach direction(s) and waypoint definitions and can be extended to the execution of non-nominal maneuvers, such as collision avoidance maneuvers. The obtained maneuver costs in terms of ΔV are promising and can be further traded-off with the maneuver time and the overall tuning of the GNC.

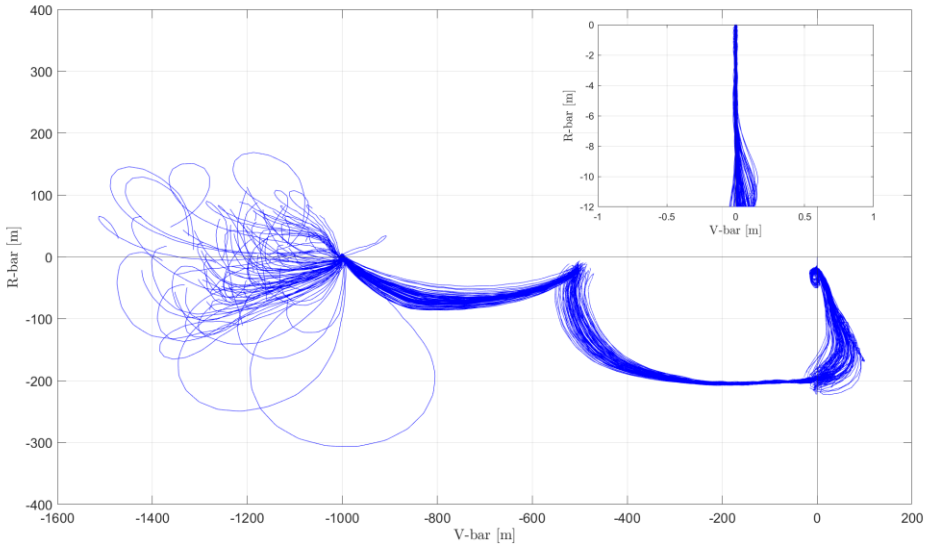

Figure 7. Relative position in Hill's frame for the combined RV-bar approach

6 CONCLUSION

This paper has presented the developments by SENER on GNC for rendezvous and docking, within the frame of internal R+D activities and the participation on ESA PoC-1 Phase 0/A. The envisioned architecture consists of an optimization-based guidance and control function, together with a cooperative optical relative navigation strategy. The requirements on the GNC performance are mainly derived from the capture requirements of the SIROM docking interface. Furthermore, the standardization objective of ESA PoC-1 requires the GNC to be robust but flexible.

The guidance and control problem was solved by application of convex programming and is integrated in a Model Predictive Control scheme, which provides further robustness and increases its accuracy and flexibility. This implementation has been greatly enabled by the in-house autocodable optimization toolbox, SOTB. The relative navigation function is addressed by formulating a cooperative architecture, based on marker-based navigation and laser rangefinder measurements for the final approach and docking, and aided by the client navigation message, transmitted through inter-satellite link. Due to the demanding GNC performance requirements, a custom data fusion architecture has been developed and implemented as a simulation prototype. Preliminary tests on this navigation architecture show great potential in terms of enhancing the relative state knowledge and, therefore, further enabling the overall GNC performance.

Within the frame of PoC-1 Phase 0/A, SENER has successfully developed the backbone in terms of rendezvous and docking GNC and tested it in simulation campaigns, for different vehicle configurations and various concepts of operations, highlighting the flexibility of the implemented strategy. Even though further developments are expected in the future, the current architecture allows meeting the capture condition, even when the mechanical interface poses demanding requirements on the GNC. It can be further expanded to account for additional maneuvers and non-nominal scenarios, such as collision avoidance maneuvers, with minor variations required. SENER has already started testing the developed GNC solution with Hardware-in-the-Loop using a robotic arm facility

and will continue to do so in the future in parallel to the further developments of the GNC architecture and algorithms.

7 REFERENCES

[1] ESA. Building the European Space Logistics Ecosystem for In-Space Transportation. Available at: https://commercialisation.esa.int/2022/09/building-the-european-space-logistics-ecosystem-for-in-space-transportation-2/. Accessed: May 2023.

[2] Viñals, J., et al. Standard Interface for Robotic Manipulation (SIROM): SRC H2020 OG5 Final Results – Future Upgrades and Application. In: International Symposium on Artificial Intelligence, Robotics and Automation in Space 2020, i-SAIRAS 2020. Oct 2020, Pasadena, California. Available: https://www.hou.usra.edu/meetings/isairas2020fullpapers/pdf/5031.pdf.

[3] Ramirez, J. and Hewing, L. Sequential Convex Programming for Optimal Line of Sight Steering in Agile Missions. In: 9th European Conference for Aeronautics and Aerospace Sciences, EUCASS 2022. DOI: https://doi.org/10.13009/EUCASS2022-7361. Jun. 2022.

[4] Martinez, A., et al. Guidance, Navigation, and Control for the autonomous rendezvous with an uncooperative tumbling target. In: ESA Clean Space Industry Days 2022. Oct. 2022, ESTEC. Available: https://indico.esa.int/event/416/contributions/7423/

[5] Clohessy, W.H. and Wilshire, R.S. Terminal Guidance Systems for Satellite Rendezvous. In: Journal of the Aerospace Sciences 27.9, pp. 653-658. 1960.

[6] Nocedal, J. and Wright, S.J. Numerical Optimization, 2nd Edition. Springer. 2006.

[7] Xie, Y., et al. Guidance, Navigation and Control for Spacecraft Rendezvous and Docking: Theory and Methods. ISBN: 978-981-15-6989-0. DOI: 10.1007/978-981-15-6990-6. Jan. 2021.

[8] Valentin, P., et al. Optimal science-time reorientation policy for the Comet Interceptor flyby via sequential convex programming. In: CEAS Space Journal. DOI: 10.1007/s12567-021-00368-2. Apr. 2021.

[9] Markley, L. and Crassidis, J. Fundamentals of Spacecraft Attitude Determination and Control. ISBN: 978-1-4939-0802-8. DOI: 10.1007/978-1-4939-0802-8. Jan. 2014.

[10] Admatis. Marker Support Navigation. Available at: https://admatis.com/msn-marker-support-navigation/. Accessed: May 2023.

[11] Nikulin, M. and Voinov, V. Unbiased Estimators and Their Applications. In: International Encyclopedia of Statistical Science. Springer Berlin Heidelberg. ISBN: 978-3-642-04898-2. DOI: 10.1007/978-3-642-04898-2_600. 2011.